Enhanced T-type calcium channel 3.2 activity in sensory neurons contributes to neuropathic-like pain of monosodium iodoacetate-induced knee osteoarthritis

Seung Min Shin, PhD[1,2], Yongsong Cai, MD, PhD[1,3],
Brandon Itson-Zoske, BS[1], Chensheng Qiu, MD[1,4],
Xu Hao, MD, PhD[1,4], Hongfei Xiang, MD, PhD[1,4],
Quinn H Hogan, MD[1,2], and Hongwei Yu, MD[1,2]

Abstract
The monosodium iodoacetate knee osteoarthritis model has been widely used for the evaluation of osteoarthritis pain, but the pathogenesis of associated chronic pain is not fully understood. The T-type calcium channel 3.2 ($Ca_V3.2$) is abundantly expressed in the primary sensory neurons, in which it regulates neuronal excitability at both the somata and peripheral terminals and facilitates spontaneous neurotransmitter release at the spinal terminals. In this study, we investigated the involvement of primary sensory neuron-$Ca_V3.2$ activation in monosodium iodoacetate osteoarthritis pain. Knee joint osteoarthritis pain was induced by intra-articular injection of monosodium iodoacetate (2 mg) in rats, and sensory behavior was evaluated for 35 days. At that time, knee joint structural histology, primary sensory neuron injury, and inflammatory gliosis in lumbar dorsal root ganglia, and spinal dorsal horn were examined. Primary sensory neuron-T-type calcium channel current by patch-clamp recording and $Ca_V3.2$ expression by immunohistochemistry and immunoblots were determined. In a subset of animals, pain relief by $Ca_V3.2$ inhibition after delivery of $Ca_V3.2$ inhibitor TTA-P2 into sciatic nerve was investigated. Knee injection of monosodium iodoacetate resulted in osteoarthritis histopathology, weight-bearing asymmetry, sensory hypersensitivity of the ipsilateral hindpaw, and inflammatory gliosis in the ipsilateral dorsal root ganglia, sciatic nerve, and spinal dorsal horn. Neuronal injury marker ATF-3 was extensively upregulated in primary sensory neurons, suggesting that neuronal damage was beyond merely knee-innervating primary sensory neurons. T-type current in dissociated primary sensory neurons from lumbar dorsal root ganglia of monosodium iodoacetate rats was significantly increased, and $Ca_V3.2$ protein levels in the dorsal root ganglia and spinal dorsal horn ipsilateral to monosodium iodoacetate by immunoblots were significantly increased, compared to controls. Perineural application of TTA-P2 into the ipsilateral sciatic nerve alleviated mechanical hypersensitivity and weight-bearing asymmetry in monosodium iodoacetate osteoarthritis rats. Overall, our findings demonstrate an elevated $Ca_V3.2$ expression and enhanced function of primary sensory neuron-T channels in the monosodium iodoacetate osteoarthritis pain. Further study is needed to delineate the importance of dysfunctional primary sensory neuron-$Ca_V3.2$ in osteoarthritis pain.

Keywords
Osteoarthritis, dorsal root ganglia, neuropathic pain, T-type calcium channel 3.2, whole-cell patch clamp

Introduction

Osteoarthritis (OA) is the most common cause of disability, largely resulted from chronic pain exacerbated by movement and loading on the joint, which is the

[1]Department of Anesthesiology, Medical College of Wisconsin, Milwaukee, WI, USA
[2]Zablocki Veterans Affairs Medical Center, Milwaukee, WI, USA
[3]Xi'an Honghui Hospital, Xi'an, Shaanxi, PR China
[4]Department of Orthopedic Surgery, Affiliated Hospital of Qingdao University, Qingdao, PR China

Corresponding Author:
Hongwei Yu, Medical College of Wisconsin, 8701 Watertown Plank Road, Milwaukee, WI, 53226-0509, USA.
Email: hyu@mcw.edu

predominant symptom in most patients with OA and often refractory to analgesia.[1] A commonly used preclinical model for OA consists of intra-articular injection of monosodium iodoacetate (MIA), an irreversible inhibitor of glycolytic enzyme glyceraldehyde-3-phosphate dehydrogenase (GAPDH),[2] into the animal joint space, which produces a joint pathology with similarities to clinical OA and significant pain-related behavior.[3,4] Knee injection of MIA is highly efficient in inactivating chondrocyte GAPDH, which results in reduced glycolysis and cell death, followed by histological features typical of OA joint damage.[3–5] The pathogenesis of chronic pain is complex and includes components of joint degeneration with cartilage loss and aggressive subchondral bone lesions and remodeling, musculoskeletal impairments, neurogenic inflammation, and neuropathic injury.[6–9]

The rat knee joint is abundantly innervated by primary sensory neurons (PSN)s that have somata located in the dorsal root ganglia (DRG) of lumbar (L) 3 to L5 levels.[10] Sensory neuron terminals have been identified throughout the joint, including the capsule, ligaments, menisci, periosteum, and subchondral bone,[11] and the majority of these joint afferents are nociceptive.[12] Studies have demonstrated that sensitization of nociceptor innervating the joint plays a crucial role in MIA joint pain pathogenesis,[13] and this process is accompanied by DRG–PSN injury, gliosis, and extensive abnormalities in peripheral sensory nervous system (PSNS), especially at the late stage of disease, leading to peripheral and central sensitization with features similar to peripheral nerve injury-induced neuropathic pain.[14] Animal studies have shown that reduction of sensory thresholds develops in the hindlimb ipsilateral, and to some degree contralateral, to the knee injured by MIA, suggesting the presence of both peripheral and central sensitization.[15] Clinical findings, including referred pain and enhanced temporal summation, additionally support the view that peripheral and central sensitization contributes to chronic OA pain.[16] Thus, injury of the PSNs with neuropathic pain-like sensitization is one of the defined mechanistic correlates of OA-associated pain in both animal models and human disease.[10,17]

T-type calcium 3.2 channels ($Ca_V3.2$), which are abundantly expressed in PSNs and their axons, determine low-threshold mechanoreceptor function, and shape neuronal firing properties, has been demonstrated in modulating chronic peripheral and central sensitization in various chronic pain conditions.[18–20] $Ca_V3.2$ expression has also been detected in osteoblasts, osteocytes, and chondrocytes.[21] Several lines of evidences support involvement of $Ca_V3.2$ activation in OA pain pathogenesis. It is reported that mechanotransduction in bone is partially mediated through T-type voltage-gated calcium channels, and $Ca_V3.2$ knockout mice display reduced cartilage damage following repetitive knee loading-induced OA.[22] Consistent with this notion, oral small molecular selective $Ca_V3.2$ inhibitor produces dose-dependent antinociception in rat MIA-induced knee-joint pain.[23] These studies verified that the aberrant $Ca_V3.2$ activation in OA pain plays an important role in pain pathogenesis; however, whether PSN-$Ca_V3.2$ activation is involved in the MIA-OA pain remains an open question.

This study was designed to investigate whether PSN-$Ca_V3.2$ activation plays a role in MIA-OA pain, focusing on the advanced stage of MIA-OA that often presents neuropathic pain-like pathology.[24,25] We here present the evidence showing that PSN-T-type channel activity was enhanced and $Ca_V3.2$ expression increased at the advanced stage of MIA-OA and that neuronal damages beyond exclusively knee-innervating PSNs, which may contribute to the pathogenesis of MIA-OA neuropathic-like pain.

Methods and Materials

Animals

Experiments were performed in adult male Sprague Dawley rats (5–6 weeks old; 125–150 g body weight) purchased from Charles River Laboratories (Wilmington, MA). Rats were housed in standard 12-h cycle lighting and were allowed ad libitum access to food and water prior to and throughout the experimental protocol. All animal procedures were reviewed and approved by the Animal Care Committee of the Zablocki VA Medical Center Animal Studies Subcommittee and Medical College of Wisconsin IACUC (Permission number: 3690–03). All efforts were made to minimize suffering and the numbers of animals used. For tissue harvest euthanasia, animals were deeply anesthetized by isoflurane followed by decapitation with a well-maintained guillotine. The numbers of rats used were detailed in the relevant sections or figure legends of the experiments.

Induction of knee OA

The MIA model of knee OA was induced in isoflurane-anesthetized animals as previously described.[26] In brief, after briefly anesthetized with isoflurane (2% v/v) vaporized in oxygen, rats received a single intra-articular cavity injection of 2 mg MIA (Sigma–Aldrich, St. Louis, MO) in 50 μl sterile 1× phosphate-buffered saline (saline) through the infrapatellar ligament of the right knee, assisted by flexed the knee at a 90° angle. Control rats received intra-articular injection of saline (50 μl).

Behavior tests

Animals were habituated in individual test compartments for at least 1 h before each testing.[27,28] Behavior

tests carried out as previously described were performed by personnel blind to the injection.

1. Weight-bearing (WB) asymmetry: An Incapacitance tester (Columbus Instruments, Columbus, OH) was used to determine hindpaw weight distribution. Rats were placed in an angled Plexiglas chamber so that each hindpaw rested on a separate force plate. The change in hindpaw weight distribution was automatically calculated by Incapacitance tester (the difference in the amount of weight (g) between the left and right limbs). Essentially, the apparatus calculates an average weight distribution over the span of 5 s, and three recordings are taken for each rat. All three recordings are then automatically averaged, and a mean score is displayed. The primary dependent measure was % weight on ipsilateral hindpaw and was determined by the formula: Weight bearings (%) = force (g) of right hindpaw/[force (g) of left hindpaw + force (g) of right hindpaw] × 100. A value of less than 50% indicates a reduction in weight borne on the ipsilateral hindlimb.

2. Mechanical allodynia: Static mechanical withdrawal thresholds (von Frey, vF) were assessed by applying the calibrated monofilaments (Patterson Medical, Bolingbrook, IL) to the plantar surface of the hindpaw. Briefly, beginning with the 2.8 g filament, filaments were applied with just enough force to bend the fiber and held for 1 s. If a response was observed, the next smaller filament was applied, and if no response was observed, the next larger was applied, until a reversal occurred, defined as a withdrawal after a previous lack of withdrawal, or vice versa. Following a reversal event, four more stimulations were performed following the same pattern. The forces of the filaments before and after the reversal, and the four filaments applied following the reversal, were used to calculate the 50% withdrawal threshold. Rats not responding to any filament were assigned a score of 25 g.

3. Mechanical hyperalgesia: Noxious punctate mechanical stimulation (Pin test) was performed using the point of a 22 g spinal anesthesia needle that was applied to the center of the hindpaw with enough force to indent the skin but not puncture it. Five applications were separated by at least 10 s, which was repeated after 2 min, making a total of 10 touches. For each application, the induced behavior was either a very brisk, simple withdrawal with immediate return of the foot to the cage floor, or a sustained elevation with grooming that included licking and chewing, and possibly shaking, which lasted at least 1 s. This latter behavior was referred to as hyperalgesic behavior, which is specifically associated with place avoidance.[29] Hyperalgesia was quantified by tabulating hyperalgesia responses as a percentage of total touches.

4. Cooling stimulation (cold): Acetone was expelled from a syringe attached to PE220 tubing to make a meniscus that was touched to the plantar surface of the hindpaw, such that the drop spread out on the plantar surface of the paw without contact of the tubing to the skin. Each hindpaw was tested three times in alternating fashion. Any withdrawal was considered a positive response.

5. Heating plantar test (heat): Heat-pain threshold of the hindpaw was determined using a device designed for the purpose of identifying thermal sensitivity (Paw Thermal Stimulator System, University Anesthesia Research & Development Group, San Diego, CA). Rats were placed on a temperature-regulated glass platform heated to 30°C and the hindpaws stimulated with a radiant heat source (50 W halogen bulb) directed through an aperture. The time elapsed from initiation of the stimulus until withdrawal (withdrawal latency) as detected by a series of photocells was measured. Each hind paw was tested four times and the withdrawal latency values averaged.

Histology and immunohistochemistry (IHC)

Following behavior testing at the fifth week after MIA injection, animals were terminally anesthetized. Tissues were used at this timepoint since this represents an advanced stage at which all articular structure and behavior changes associated with OA application have become fully developed.[30,31]

1) Knee histopathological analysis: The knee joints from the tibia to the distal metatarsal including the tarsal joint were resected and fixed with 10% neutral-buffered formalin for 48 h at room temperature. The fixed specimens were decalcified in Immunocal (ThermoFisher, Waltham, MA) for two weeks and embedded in paraffin. Sections of the tissue specimens were acquired from the paraffin blocks at 5 µm thickness, deparaffinized and rehydrated in the order of xylene and series of absolute to 50% alcohol. The rehydrated sections were stained with hematoxylin and eosin (H&E) for the observation of morphological changes in the articular tissues. Images of knee joint histology were captured using a Keyence BZ-X800 microscope (Keyence Corporation, Itasca, IL).

2) Immunohistochemistry (IHC): DRG and lumbar spinal cord (SC) segments were dissected, post-fixed in 10% buffered formalin, and processed for paraffin embedding and sectioning. IHC double staining was performed to characterize the distribution of target molecules in tissue sections, as previously described.[32] In brief, after deparaffinized and hydrated, sections were treated by heat-induced antigen epitope retrieval in

Table 1. Primary antibodies and IgG controls used in this study.

Antibody	Host	Supplier/Cat#/RRID[b]	Dilution
IB4		LF/I21413	1.0 µg/ml
$Ca_V3.2$[a]	Rabbit polyclonal	Alomone/ACC025/AB2039781	1:500 (IHC), 1:1000 (Wb)
ATF3	Rabbit polyclonal	SCB/SC188	1:200 (IHC), 1:800 (Wb)
Iba1	Rabbit polyclonal	Wako/019-19741	1:1000 (IHC)
GFAP	Rabbit polyclonal monoclonal	Dako/Z0334	1:500 (IHC)
Tubb3	Mouse monoclonal monoclonal	SCB/sc-80016	1:400 (IHC), 1:1000 (Wb)
GAPDH	Mouse monoclonal monoclonal	Sigma/SAB1403850	1:2000 (WB)
IgG control	Mouse	LF/31903	1:100~400
IgG control	Rabbit	LF/MA5-16384	1:100~1000

$Ca_V3.2$: T-type voltage-gated calcium channel 3.2; IB4: isolectin IB4; ATF3: activated transcriptional factor 3; Iba1: ionized calcium-binding adapter molecule 1; GFAP: glial fibrillary acidic protein; Tubb3: β3-Tubulin; GAPDH: glycolytic enzyme glyceraldehyde-3-phosphate dehydrogenase; IgG: immunoglobulin G; IHC: immunohistochemistry; WB: weight bearing.
[a]Antigenic peptide: CHVEGPQERARVAHS, corresponding to amino acid residues 581–595 of rat $Ca_V3.2$ intracellular loop between domains D1 and D2.
[b]LF, Life Technologies, Carlsbad, CA; Alomone, Alomone Labs, Jerusalem, Israel; SCB, Santa Cruz Biotechnology, Santa Cruz, CA; Wako, Richmond, VA; Dako: Carpinteria, California; Sigma, Sigma–Aldrich, St Louis, MO.

10 mM citrate buffer, pH 6.0. Sections were first immunolabeled with the selected primary antibodies overnight at 4°C (Table 1). A well-characterized $Ca_V3.2$ antibody was used, which is raised against a rat $Ca_V3.2$ peptide, corresponding to amino acid residues 581–595 of rat $Ca_V3.2$ intracellular loop between domains D1 and D2 and its specificity to detect the target has been verified by IHC on $Ca_V3.2$ knockout tissue.[33] All antibodies were diluted in 1x PBS, containing 0.05% Triton X-100 and 3% bovine serum albumin (BSA). Normal immunoglobulin G (IgG from the same species as the first antibody, Table 1) was replaced for the first antibody as the negative controls. The appropriate fluorophore-conjugated (Alexa 488 or Alexa 594, 1:2000) secondary antibodies (Jackson ImmunoResearch, West Grove, PA) were used to reveal immune complexes. The sections were washed three times for 5 min each with PBS containing 0.05% tween-20 between incubations. To stain nuclei, 1.0 µg/ml Hoechst33342 (Hoechst, ThermoFisher) was added to the secondary antibody mixture. The sections were examined, and images captured using a Nikon TE2000-S fluorescence microscope (El Segundo, CA) with filters suitable for selectively detecting the green and red fluorescence using a QuantiFire digital camera (Optronics, Ontario, NY). For double label colocalization, images from the same section but showing different antigen signals were overlaid. Quantification of the percentage of ATF3-positive DRG neurons was determined by counting the number of ATF3 immunoreactive (IR) and non-IR neurons with visible nuclei marked by Hoechst, as previously described.[34] For quantification of spinal dorsal horn (SDH) $Ca_V3.2$ immunostaining, the Image J (ImageJ v.1.46, National Institutes of Health) was used to quantify changes in immunolabeled fluorescent densities as described previously,[35] with some minor modifications. In brief, the sections with

symmetrical width of DHs throughout the mediolateral axis were used for measurement, and the upper and lower threshold optical densities were adjusted to encompass and match the immunoreactivity (IR) that appears in red. A standardized rectangle was first positioned over laminae territory throughout the mediolateral axis on the contralateral DH. The area and density of pixels within the threshold value representing IR were calculated and the integrated density was the product of the area and density. The same box was then moved to the corresponding position on the opposite DH and the integrated density of pixels within the same threshold was again calculated. Comparisons of both sides of DHs were made only within the same sections and density values on the ipsilateral side were expressed as a percent of the contralateral side, providing an estimate of fold change for each section.

Immunoblots

DRG and SDH tissues at the fifth week after MIA or saline injection were harvested. The lysates from DRG and SDH tissues were extracted using 1× RIPA buffer (20 mm Tris-HCl pH 7.4, 150 mm NaCl, 1% Nonidet P-40, 1% sodium deoxycholate, 0.1% SDS, with 0.1% Triton X100 and protease inhibitor cocktail). Protein concentration was determined by using the Pierce BCA kit (ThermoFisher). Equivalent protein samples were size separated using 10% or 4%–20% SDS-PAGE gels (Bio-Rad Laboratories, Des Plaines, IL), transferred to Immun-Blot PVDF membranes (Bio-Rad) and blocked for 1 h in 5% skim milk. The blots were cut into two halves along protein size around 70 KDa.[36] then subsequently incubated overnight at 4°C with appropriate antibodies. IR proteins were detected by Pierce enhanced chemiluminescence (ThermoFisher) after incubation for 1 h with HRP-conjugated second antibodies (1:5000,

Bio-Rad). The densitometry of bands of interests was analyzed using ImageJ v.1.46. Ratios of the band density of the target proteins to GAPDH band density were calculated and the percentage changes of target proteins in the experimental samples compared with those from the control samples.[37,38]

Whole-cell patch-clamp recording of T-type Ca^{2+} channel current on dissociated DRG neurons

Whole-cell patch-clamp recording on dissociated DRG neurons was performed, as described previously.[39] In brief, the DRG (L3, L4, and L5) were rapidly harvested from the isoflurane-anesthetized animals and were incubated in 0.01% blendzyme 2 (Roche Diagnostics, Madison, WI) for 30 min followed by incubation in 0.25% trypsin and 0.125% DNase for 30 min, both dissolved in DMEM/F12 with glutaMAX (ThermoFisher). After exposure to 0.1% trypsin inhibitor and centrifugation, the pellet was gently triturated in culture medium containing Neural basal media A (ThermoFisher) plus 0.5 μm glutamine. Dissociated cells were plated onto 5% laminin-coated glass coverslips (ThermoFisher) and maintained at 37°C in humidified 95% air and 5% CO_2 for 2 h and were studied no later than 6–8 h after harvest.

Electrophysiological recordings on the DRG neurons were performed in a blind manner where the electrophysiologist was not aware of the treatment (MIA or saline). Voltage-induced currents flowing through Ca^{2+} channels were recorded using an extracellular solution containing (in mM): 2 $BaCl_2$, 4-aminopyridine 1, 10 HEPES, 140 tetraethylammonium chloride (TEACl), pH of 7.4, with an osmolarity of 300 mOsm. To selectively record T-type low-voltage activated (LVA) calcium currents (I_{Ca}), neurons were preincubated in a Tyrode's solution with 0.2 μM ω-conotoxin GVIA, 0.2 μM nisoldipine, and 0.2 μM ω-conotoxin MVIIC for at least 30 min. ω-conotoxin GVIA irreversibly blocks N-type I_{Ca}, and ω-conotoxin MVIIC irreversibly blocks P-/Q-type I_{Ca}. The concentrations used were saturating in preliminary experiments.[39] Any residual high-voltage activated (HVA) I_{Ca} following incubation of HVA calcium channel blockers was eliminated by using fluoride in the internal pipette solution.[39,40] The fluoride (F^-)-based internal solution, which was used in all experiments examining LVA I_{Ca}, contained (in mM): 135 tetra-methyl ammonium hydroxide (TMA-OH), 10 EGTA, 40 HEPES, and 2 $MgCl_2$, adjusted to pH 7.2 with hydrofluoric acid. A selective and reversible T-type Ca^{2+} channel blocker, TTA-P2 (3, 5-dichloro-N-[1–(2,2-dimethyl-tetrahydropyran-4-ylmethyl)-4-fluoro-piperidin-4-ylmethyl]-benzamide, Alomone Labs, Jerusalem, Israel),[40] was used to confirm the T-type I_{Ca}.[39] Patch pipettes, ranging from 2–4MΩ resistance, were formed from borosilicate glass (King Precision

Glass Co., Claremont, CA) and fire polished. Recordings were made with an Axopatch 700B amplifier (Molecular Devices, Downingtown, PA). Signals were filtered at 2 kHz and sampled at10 kHz with a Digidata 1440 A digitizer and pClamp10 software (Molecular Devices). Series resistance (5–10 MΩ) was monitored before and after the recordings, and data were discarded if the resistance changed by 20%. After achieving the whole cell recording, capacitance and series resistance were compensated accordingly. Leak currents were digitally subtracted using a P/4 leak subtraction protocol. Voltage protocols consisted of 400-ms square-wave commands from a holding potential of −90 mV for LVA to +60 mV in 10mV increments with 5 s intervals between steps. The peak T-current was measured after subtracted from the current at the end of the depolarizing test potential to avoid contamination with residual HVA currents.[40] Measured inward current was normalized by membrane capacitance, which results in a T-channel I_{Ca} density corrected for cell size (pA/pF). To determine the current–voltage (I–V) relationship of voltage-dependent activation, the peak I_{Ca} densities during each voltage command step were fitted to a smooth curve with a Boltzmann equation: $I = G_{max}(V-E_{rev})/[(1+\exp[(V-V_{50})/k)])]$, which provided the maximum conductance (G_{max}). Normalized activation curves were fitted with a Boltzmann equation $G/G_{max} = 1/(1+\exp(V_{50}-Vm)/k)$, where G was calculated as follows: $G = I/(Vm-E_{rev})$. The steady-state inactivation curves were fitted with $I/Imax = 1/(1+\exp(V_{50}-Vm)/k)$. In all of the equations, V_{50} denotes the half-activation and half inactivation potentials, Vm is the membrane potential, Erev is the inversion potential, k is the slope factor, G is the conductance, and I is the current at a given Vm; G_{max} and I_{max} are the maximum conductance and current, respectively.

Subepineural sciatic nerve injection

In this experiment, injection was performed in a blinded manner by which the operator was unaware of the content of the injectate. TTA-P2 was dissolved in dimethyl sulfoxide (DMSO) to a 100 mM stock solution, stored at −20°C, diluted to desired concentrations with saline just before use. It is reported that half of the total cross-section inside the sciatic nerve (SN) epineurium in human consists of non-neural connective tissue.[41] Rats at five weeks post MIA knee OA induction were randomized into two groups, and subepineural sciatic nerve injection (SSNI) was performed as previously described,[42,43] with some modification. In brief, after appropriate anesthesia was obtained by inhalation of 2% isoflurane, the SNs were exposed by lateral incision of the middle thighs and division of the superficial fascia and muscle. Then 100 μl of the test dose at TTA-P2

(containing 0.01% DMSO) was injected slowly, directly into subepineural space (beneath the clear fascia surrounding the nerve but outside the perineurium) through a 33-gauge needle, proximal to the sciatic bifurcation. The needle remained in place at the injection site for 1 additional min, before it was slowly removed. The TTA-P2 dose used were saturating in preliminary experiments. Control rats received SSNI with 100 μl saline containing 0.01% DMSO. The superficial muscle layer was sutured with 4–0 silk, and the wound was closed with metal clips. Ipsilateral hindpaw mechanical allodynia (vF) and hyperalgesia (Pin) as well as WB asymmetry were tested before and 15, 30, 45, 60, 120, and 180 min after animal recovered after injection of TTA-P2 or vehicle.

Statistics

All statistical analysis was performed using Prism program (GraphPad Software, San Diego, CA). Data were expressed as means ± SEM. A probability of $p < 0.05$ was considered as statistically significant. Behavioral changes over time in each group were analyzed by repeated measures parametric two-way ANOVA for von Frey, WB, and heat testing with post hoc multiple comparison by Tukey's test, and non-parametric Friedman's ANOVA for pin and cold testing with Dunn's test for post hoc analysis. Differences of ATF3 immunopositivity, patch recording T-channel peak I_{Ca} density, and immunoblot $Ca_V3.2$ protein levels between groups were compared with a two-tailed, unpaired t test.

Results

MIA OA knee histopathology and pain behavior

Histological examination of H&E staining of knee joints 35 days following intra-articular injections demonstrate that saline-treated knees have intact and smooth articular surfaces. MIA-treated knees displayed typical structural joint damage 35 days after MIA knee cavity injection as reported,[25,44] showing a considerable loss of articular cartilage surrounding the subchondral bone along the joint, combined with bone marrow lesions and collapse of subchondral bone (Figure 1(a-a1) and (b-b1), $n = 4$ per group) which has
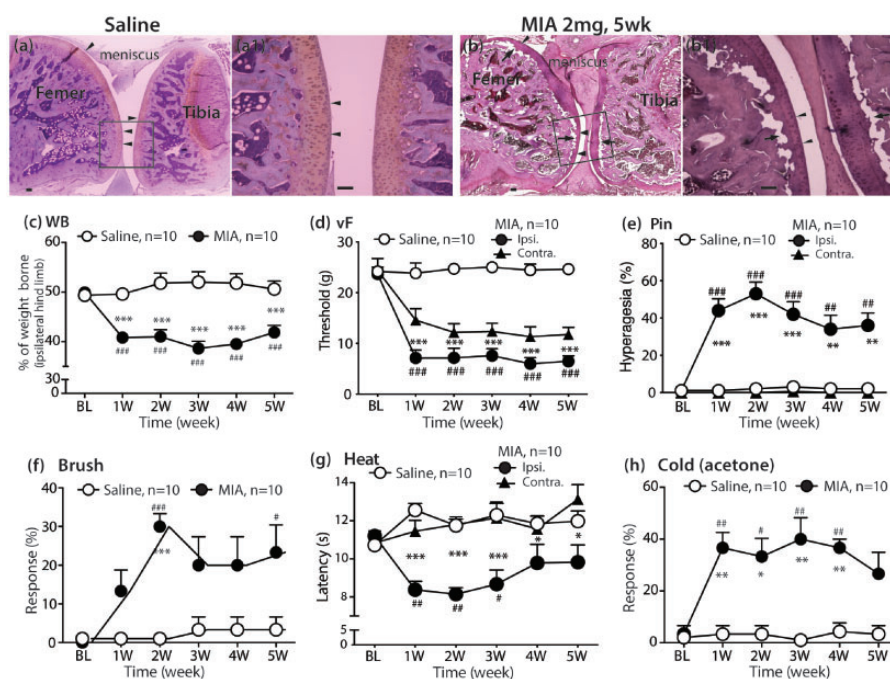

Figure 1. MIA OA histopathology and pain behavior. H&E stained sagittal section of saline-injected knee with femoral condyle at the left and tibial condyle at the right, showing full-depth normal cartilage and normal subchondral bone structure (a), and the region within the square shown at high magnification (a1). OA-like findings in a representative H&E-stained sagittal section of knee five weeks after MIA (2 mg) injection, showing articular cartilage loss (arrowheads), reduced chondrocyte numbers, subchondral bone collapse (arrows) (b), and the region within the square shown at high magnification (b1). Scale bar: 100 μm for all. Intra-articular knee injection of 2 mg MIA-induced pain behavior measured as ipsilateral hindlimb WB asymmetry (c), increased responsiveness to innocuous mechanical stimulation (von Frey, d), noxious pin touch (e), and dynamic innocuous mechanical stimulation (brush, f), and reduced thresholds to heat (g) and cold (h) stimulation. Repeated measures two-way ANOVA with Bonferroni post-hoc for WB, von Frey and heat; and nonparametric analyses by Friedman's test with Dunn's post hoc for Pin, brush, and cold. #$p < 0.05$, ##$p < 0.01$, and ###$p < 0.001$ for comparison to baseline (BL) and *$p < 0.05$, **$p < 0.01$, and ***$p < 0.001$ for comparison between groups after MIA or saline knee injection.

been reported to be associated with the resultant pain behavior.[45]

All of the rats that received 2 mg MIA knee injection exhibited asymmetric hindlimb weight bearings (WB) throughout the course of the study, confirming OA knee spontaneous pain development following MIA knee injection. Specifically, following MIA knee injection, animals displayed significant reduction of WB on the ipsilateral hind limb compared to their respective saline control with weight symmetry. The magnitudes of WB reduction were similar to previous reports[25,26] and persisted during the entire five weeks after OA induction. In addition to pain on loading (WB), all animals injected with MIA developed consistent and significant ipsilateral mechanical allodynia to normally innocuous mechanical stimulation (brush and vF) and hyperalgesia to noxious mechanical stimulation (Pin), as well as hypersensitivity to heat and acetone (Figure 1(c)–(h)). These were evident by one week and persisted for the entire five weeks for which the MIA-injected animals were tested. Mechanical allodynia (vF) but not mechanical hyperalgesia or thermal stimulation was also observed on the contralateral hindpaw (Figure 1(d), (e) and (g)). These data show that MIA induces significant local (knee joint) and remote (hindpaw) sensitization. Conceivably, the mechanical and thermal stimulated hindpaw withdraw during tests can also facilitate knee local pain because of knee movement triggered by repeated stimulation at hindpaw plantar. These findings, together with previous observations by others,[46] indicate that MIA-induced OA, in addition to direct unilateral knee damage, induces central sensitization that can also spread sensitization to the contralateral hindpaw.

MIA-OA induces extensive PSN injury and inflammatory gliosis in PNS and SDH

Increased activating transcription factor 3 (ATF3) expression is a selective marker of neuronal damage.[47] An increase of ATF3 expression in the PSNs is a robust finding in peripheral nerve injury-induced neuropathic pain and also a common phenomenon of MIA OA pain models.[25] Here, we analyzed ATF3 expression by IHC in the lumbar DRG harvested at the five weeks post MIA injection ($n = 4$ rats). This showed clearly increased ATF3 immunopositivity in the majority of the neurons from the sections of all L3, L4, and L5 DRG, while weak ATF3-positivie neurons were visualized in ~10% neurons from controls (Figure 2(a)–(e)). ATF3 is not thought to be expressed during inflammation,[48] so these suggest that PSN damage was a pathological feature at the late stage after 2 mg MIA treatment and occurred in a broad segment of lumbar DRG. It is well-characterized that MIA injection induces inflammatory response not only in the knee but also along the

peripheral sensory pathways and SDH,[26] which can also mediate neuronal injury.[7,25] Glial cells in the sensory pathways can respond to peripheral tissue damage, releasing factors that interact with neurons to regulate their function.[49] We next determined the inflammatory gliosis in PNS and SDH five weeks after MIA injection by IHC, using antibodies of GFAP to selectively identify DRG satellite glial cells (SGCs) and SDH astrocytes, as well as Iba1 to selectively identify microglia (Figure 2(f)–(o)). Our results showed clear increases of both GFAP- and Iba1-positive glial cell populations, indicative of extensive gliosis in the PNS and SDH ipsilateral to MIA, in agreement with previous findings that showed proliferation/activation of glial cells in PNS and SDH after MIA joint injection.[50,51] Data suggest that neuronal damage and inflammatory responses are beyond merely knee-innervating PSNs but rather involves widespread changes in sensory neurons.[25,52]

MIA-OA increases T-type Ca^{2+} channel current in PSNs

Abundant data support an important role of Ca$_V$3.2 in generating pain states including various inflammatory and neuropathic pain models.[20] We next focused on examining whether T-type Ca^{2+} channel activity was altered in the MIA OA model, using electrophysiological recording of T-channel current (I$_{Ca}$) of PSNs dissociated from DRGs five weeks after MIA injection. LVA current was isolated by blocking HVA currents with specific toxins.[39] We chose to record from small- to medium-size PSNs ($<40\,\mu m$ soma diameter) because these are likely nociceptors and have T-type currents under normal conditions.[53,54] Since ATF3 immunostaining indicated neuronal damage in the majority PSNs in L3, L4, and L5 DRG at the late stage after 2 mg MIA injection, whole-cell patch-clamp was conducted on the randomly selected PSNs dissociated from L3, L4, and L5 DRG, individually ($n = 4$ for each L3, L4, and L5 DRG from four rats per group). To determine the expression of T-type currents, we set holding potentials (V_h) to $-90\,mV$ and recorded currents during depolarizations to test potentials (V_t) of -80 to $+60\,mV$ in 10mV increments. The resulting inward currents showed a crossing pattern of T-type channels (Figure 3(a) and (b)). Neurons expressing LVA currents represented 44% (60 out of 137 cells recorded) of the total population in saline vs 47% (60 out of 128 cells recorded) in MIA neurons. Application of $5\,\mu M$ TTA-P2 inhibited >90% of the current, confirming that these were currents through the T-type channel. Current–voltage (I–V) relationships showed that average I$_{Ca}$ intensity was increased >2 fold for neurons from L3, L4, or L5 DRG of MIA animals compared to the saline-injected groups, across a wide range of test potentials (-80 to $+20\,mV$) (Figure 3(c)–(f)). No significant
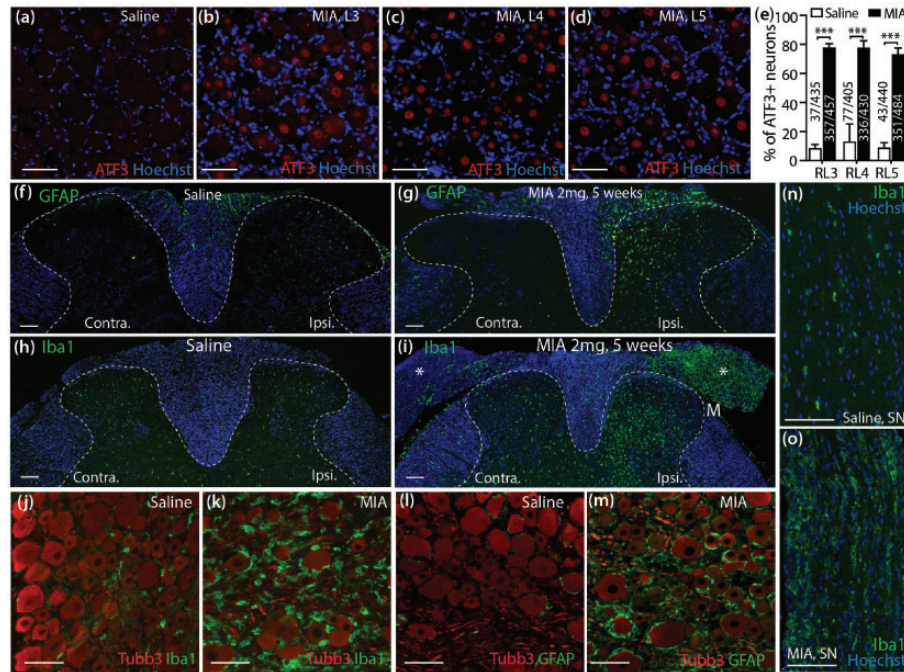
Figure 2. IHC characterization of PSN damage and inflammation. (a-e) shows representative IHC images stained for ATF3 (red) and counterstained by Hoechst on DRG sections five weeks after saline (a) or 2 mg MIA injection (L3, b; L4, c; and L5, d), with bar chart (e) showing the quantitative comparison of the percentage of ATF3-positive neurons in L3 to L5 DRG between saline and MIA groups ($n = 3$ DRG per group). Values are ATF3-positive number of total determinations (neurons with visible nuclei); *** denotes $p < 0.001$, two tailed unpaired Student's t tests. (f–m) show representative IHC staining for GFAP and Iba-1 on lumbar SC and DRG sections. In comparison with controls that display symmetrically scattered distribution of GFAP-positive astrocytes (green) and Iba1-positive microglia (green) in the lumbar SDH (f, h), marked gliosis for both astrocytes and microglia are seen ipsilateral to MIA OA in the SDH (g, i), with asterisks in panel (i) indicating microgliosis in dorsal root ipsilateral to MIA injection. In the DRG, minimal staining is evident for Iba-1 and GFAP after saline knee injection (j, l), but shows abundant positive staining after MIA knee injection for Iba-1 (k) and GFAP (m). Microgliosis is also evidence in sciatic nerve (cf. panel n of control and panel o of MIA). Scale bar: 50 μm for all.

alteration on the voltage-dependent activation and steady-state inactivation properties was observed (Figure 3(g)–(h)). Together, the results suggest that T-type channel activity was significantly enhanced after MIA compared to the control group; and this effect, since the activation and inactivation kinetics were spared, was unlikely due to the change in T-channel biophysical properties but might be resulted from the increased Ca$_V$3.2 expression that can lead to enhanced channel activity.[18,55]

MIA-OA induces increased Ca$_V$3.2 expression in nociceptive pathways

We next examined and compared Ca$_V$3.2 protein expression in DRG and SDH between MIA- and saline-treated animals at the advanced stage (35 days) of MIA OA by IHC and immunoblots. In the control DRG, high Ca$_V$3.2 IR signals were preferably detected in small- and medium-sized PSNs co-stained with IB4 and CGRP (Figure 4(a) and (b)). High Ca$_V$3.2-IR was also detected in the IB4, CGRP, pCaMKII, and Tubb3 positive axonal fibers in SN (Figure 4(c), (e), (f), (g)), as well

as IB4 (Figure 4(d)) and Tubb3 (Figure 4(h)) positive dermal nerve bundles of hindpaw glabrous skin. IHC patterns of Ca$_V$3.2-IR in SC, DRG, and SN were in agreement with previous reports.[33,55,56] Quantitative comparison of DRG-Ca$_V$3.2 protein levels was performed by western blots. Since neuronal damages with enhanced PSN T-channel I_{Ca} density were evident in multiple segments of lumber DRG derived from MIA-treated animals, pooled L3-L5 DRG were used to prepare samples for immunoblots. Results showed that Ca$_V$3.2 protein levels in the pooled L3-L5 DRG were significantly increased in the MIA-OA group compared to control samples (Figure 4(i)). Since the DRG tissues harvested contained adjacent roots and spinal nerve attached, the increased Ca$_V$3.2 protein levels reflected increased Ca$_V$3.2 in both PSNs and their axons. IHC examination on lumbar SC cross-sections showed fairly symmetric Ca$_V$3.2-IR preferably in the neurons of ipsilateral and contralateral SDH of saline-treated animals (Figure 5(a-a1)), whereas the Ca$_V$3.2-IR of ipsilateral DH (Figure 5(b)) that showed microgliosis (Figure 5 (c)) in MIA-treated rats was apparently increased compared to the contralateral site (Figure 5(a) and (a1)), and
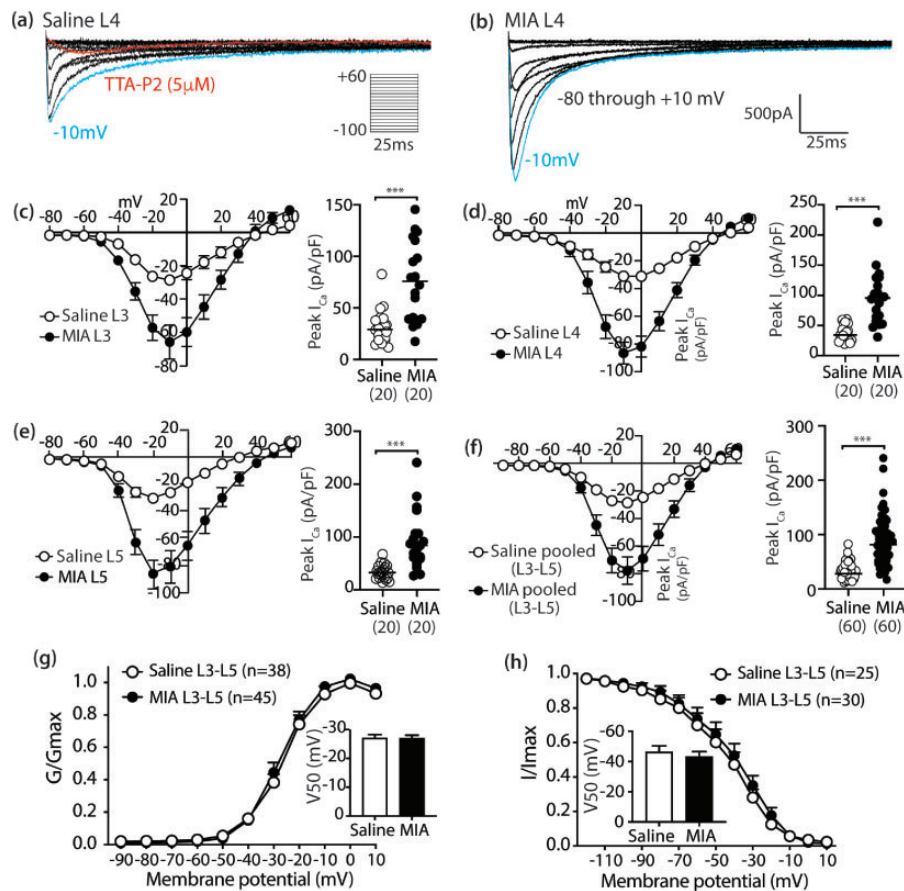
Figure 3. Enhanced T-type Ca^{2+} current in PSNs after MIA treatment. Representative traces of T-type I_{Ca} from L4 PSNs dissociated from the saline (a) and MIA-treated rat (b) five weeks after injection. I_{Ca} is evoked by command voltage steps from -90 mV (holding potential) to a test potential from -80 to $+60$ in 10 mV increments. Scatter and line plots show I–V relationships of the grouped data in the saline (open circles) and MIA groups (filled black circles) recorded in the small- and medium-sized PSNs dissociated from L3 (c), L4 (d), and L5 (e) DRG, as well as L3–L5 pooled data (f); with scattered dot plots with medians on the right of each panel summarized peak I_{Ca} density; *** denote $p < 0.001$ by two-tailed unpaired Student's t tests for comparison between saline and MIA groups, respectively. The number in each bracket below x axis is the PSN numbers recorded per group. The plots (g and h) show the voltage-dependent activation and steady-state inactivation curves in two groups, with insets showing half activation and half inactivation, respectively.

this was verified by quantification of Ca$_V$3.2 immunolabeled fluorescent densities (Figure 5(d) to (f)). Quantitative comparison of Ca$_V$3.2 protein levels by western blots verified $\sim$2 fold higher of Ca$_V$3.2 in the ipsilateral DH than that of contralateral DH (Figure 5(g)). Together, these experiments demonstrate that MIA-OA induces increased Ca$_V$3.2 expression in nociceptive pathways including PSNs and their axons and DH neurons, which may have implications for promotion of chronic pain, and consequently, blocking Ca$_V$3.2 channels should attenuate the pain behavior.

SN injection of TTA-P2 attenuates mechanical hypersensitization and WB asymmetry

To further investigate whether enhanced Ca$_V$3.2 in the PSNS after MIA knee injection contributed to pain behavior, we evaluated the effects of ipsilateral SSNI

of TTA-P2, a potent and selective blocker of T-channels and antinociceptive agent, on mechanical allodynia and hyperalgesia, as well as WB asymmetry in MIA rats. In this experiment, TTA-P2 effects on neuropathic pain-like sensitization were evaluated at day 35 after MIA injection, an advanced stage of knee joint damage with established pain behavior. The vF and Pin testing thresholds as well as WB asymmetry at day 35 after MIA injection, before SSNI TTA-P2 were measured as the treatment baseline ($n = 5$ rats). Results showed that a single delivery of 100 μg TTA-P2 to PNS by SSNI induced fast analgesic effects, and the peak effects by vF, Pin, and WB tests were achieved 30 min post injection, displaying completely normalized innocuous mechanical allodynia, hyperalgesia aversion, and WB symmetry; and the effects reduced to treatment baseline levels 2 h post-administration, compared to saline injected group (Figure 6(a)–(c)). No abnormal
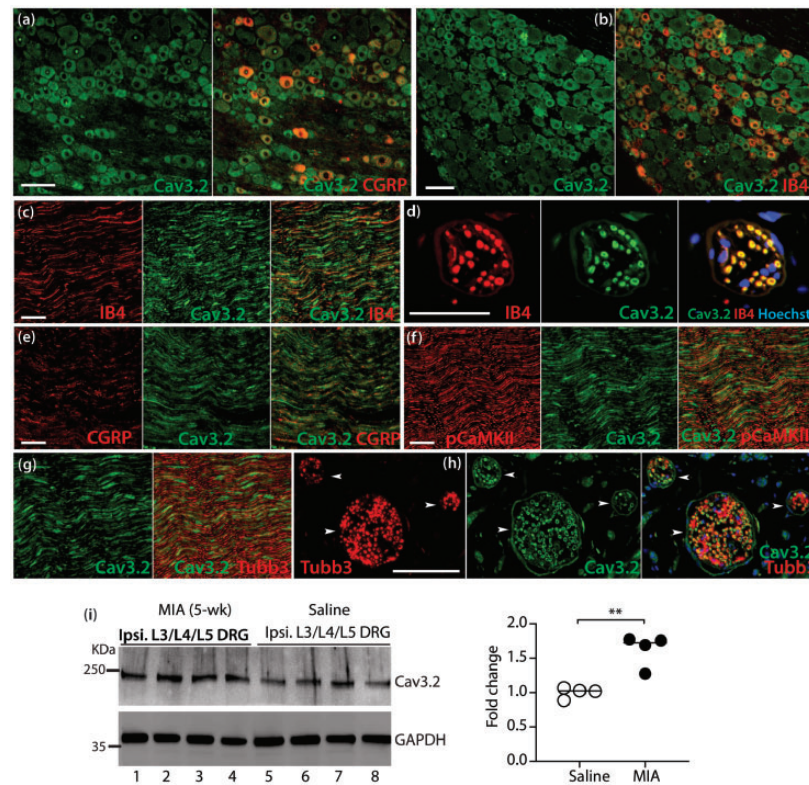
Figure 4. Increased expression of $Ca_V3.2$ in DRG of MIA OA pain rats. Representative IHC montage images show that $Ca_V3.2$-IR (a, b, green) and merged images of $Ca_V3.2$ colabeled with CGRP (red) or IB4 (red) on the sections from naïve L4-DRG. Representative montage IHC images show that $Ca_V3.2$-IR (c–h) and merged images $Ca_V3.2$ colabeled with IB4 (c, sciatic nerve; d, dermal nerve bundle), CGRP (e, sciatic nerve), pCaMKII (f, sciatic nerve), or Tubb3 (g, sciatic nerve; h, dermal nerve bundle, pointed by arrowheads). Scale bar: 50 µm for all images. Quantitative comparison of $Ca_V3.2$ expression in DRG tissues between MIA and saline groups were performed by Western blots (i) and scattered dot plots with medians in the right summarizes the grouped data; ** denote $p < 0.01$ by two-tailed unpaired Student's *t* test.

ambulation was noted for animals injected with TTA-P2 during the testing period. These data indicate that selective block of $Ca_V3.2$ channels in the PNS leads to alleviation of mechanical hypersensitivity and WB asymmetry, suggesting that $Ca_V3.2$ channels likely play a role in hypersensitivity, at least, in the advanced stage of MIA OA pain.

Discussion

In this study, the involvement of PSN-T-type Ca^{2+} channel dysfunction at the late stage of MIA knee OA pain was demonstrated by several experimental evidence: (1) PSN-T-type ICa is significantly enhanced in L3-L5 DRG ipsilateral to MIA-OA, (2) $Ca_V3.2$ expression is increased in spinal dorsal horn and PSNs and their axons, and (3) PNS block of $Ca_V3.2$ function alleviates hindpaw mechanical allodynia and hyperalgesia, as well as WB asymmetry in MIA animals. Thus, our findings provide evidence linking enhanced PSN-$Ca_V3.2$ channel activity to MIA-OA pain perception during the late

stage. Whether dysfunctional PSN-$Ca_V3.2$ is involved in the early inflammatory stage of MIA OA is not examined by this study.

The $Ca_V3.2$ is the predominant isoform of the T-type Ca^{2+} channel family, consisted of $Ca_V3.1$, $Ca_V3.2$, and $Ca_V3.3$, found in PSNs. $Ca_V3.2$ channels that modulate the function of peripheral and central nociceptive pathways by influencing peripheral sensory perception, neuronal excitability, and SC synaptic plasticity and neurotransmitter release.[18] Elevated expression and/or enhanced functionality of $Ca_V3.2$ channels have been well-defined,[20] in overall, a range of painful conditions across a variety of animal models, including inflammatory pain,[57,58] neuropathic pain,[59,60] diabetic peripheral neuropathic pain,[61–63] chemotherapy-induced peripheral neuropathy,[64] and postsurgical pain model (i.e. paw incision).[53] Activation of $Ca_V3.2$ channels following nerve damage in these models play critical roles in generating peripheral and central sensitization manifesting as pain hypersensitivity. An increased $Ca_V3.2$ activity that underlies the OA pain pathology is implicated;[22,23]
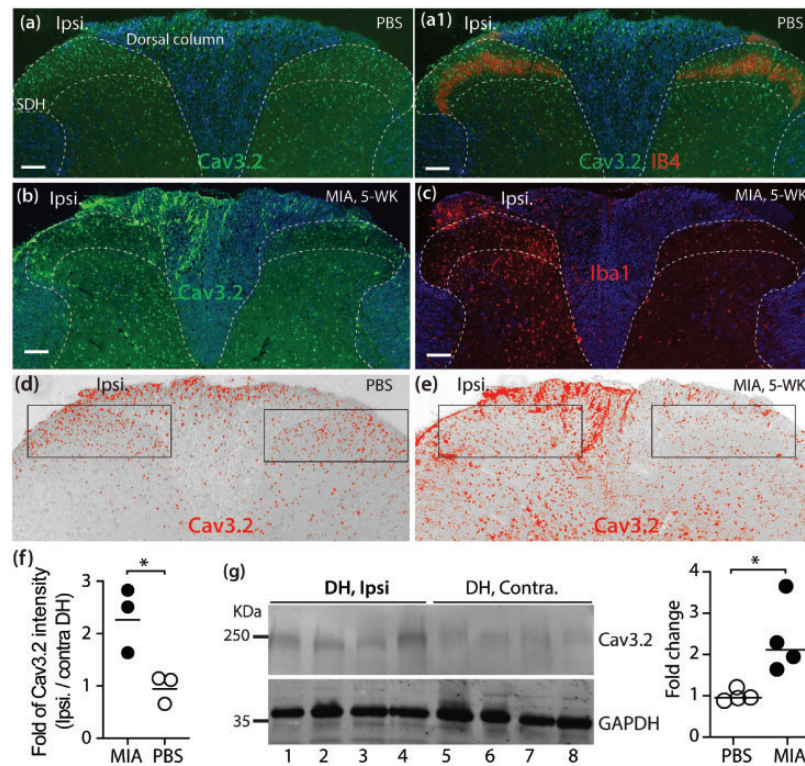
Figure 5. Increased expression of $Ca_V3.2$ in DH of MIA OA pain rats. Representative IHC montage images of $Ca_V3.2$-IR (a, green) and merged image of $Ca_V3.2$ colabeled with IB4 (a1, red) show that $Ca_V3.2$ is symmetrically distributed in the bilateral SDH of saline-treated rat. $Ca_V3.2$-IR in DH and dorsal column regions is apparently increased (b), parallel with the increased Iba1-labeled microglia (c) in the ipsilateral (ipsi.) DH of MIA-treated rat. White dashed lines outline the approximate DH and SDH with white matter pseudocolored in blue. Scale bar: $100\,\mu m$ for all. DH $Ca_V3.2$ immunolabeled fluorescent densities of saline (a) and MIA (b) were inverted, the upper and lower threshold optical densities of $Ca_V3.2$ signals adjusted to encompass and match the IR that appears in red (d) and (e), respectively; and quantified as described in Method. The rectangles (d and e) positioned over laminae territory throughout the mediolateral axis on the contra. and ipsi. DHs. The integrated density (product of area and density) calculated, and fold change (ipsi./contra.) summarized in panel (f). Quantitative comparison of $Ca_V3.2$ protein levels in DH between ipsilateral and contralateral sites was performed by Western blot. The images (g) and scattered dot plots with medians in the right of (g) summarize of the grouped data; * denote $p < 0.05$ by two-tailed unpaired Student's t test.

however, less is known about the expression and functional changes of $Ca_V3.2$ in the nociceptive pathways in the MIA-induced OA pain. Our data demonstrate increased $Ca_V3.2$ expression with enhanced function at the late stage after MIA injection, and neuropathic-like injury in PSNs can also be proposed by the demonstration of increased ATF3 IR in PSNs and extensive microgliosis in PNS. It is reported that, approximately, 5% of all DRG neurons in rat innervate knee, and most of them are from L3 and L4 DRG while less L5-DRG neurons innervate knee.[44] The increased patterns of the PSN-$Ca_V3.2$ and ATF3 changes as we observed indicated a significant percentage of sensory neurons from L3 to L5 DRG were injured during late stage of MIA OA. This may suggest sensory neuron injury beyond exclusive sensitization of knee innervating PSNs,[65] and these comorbidities of knee- and non-knee-innervating PSN injury may significantly relate to MIA OA pain

pathogenesis and influence the disease course. This observation is consistent with pain referred to other areas beyond the joint at the OA advanced stage, as reported in OA animal models showing both articular- and hindpaw-PSN sensitization[7,25,66] and in patients.[7,24,67]

Our experiments did not investigate the mechanism of upregulation of PSN-$Ca_V3.2$ in MIA OA pain, but this could include MIA OA-associated inflammatory responses and injury along the nociceptive pathway. It is known that PSN injury and microgliosis in PNS and SC are the hallmarkers of nerve injury-induced painful neuropathy, and the infiltration and activation of inflammatory cells can induce sensory neuron damage,[47] which correlates mechanistically to $Ca_V3.2$ dysfunction.[59,60,68] These pathological characteristics also occur in the advanced stage of MIA OA pain, as shown in this study and reported from the others.[25]
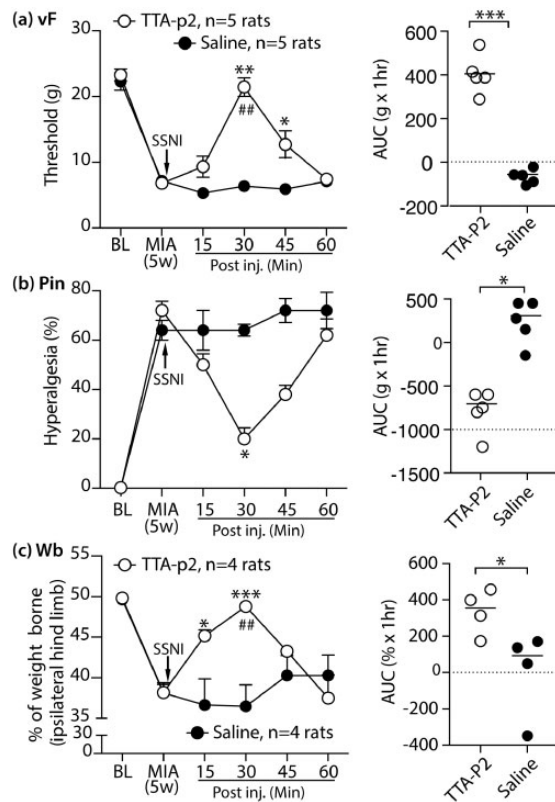
Figure 6. Reversal of mechanical pain behavior and weight-bearing asymmetry by sciatic nerve application of TTA-P2. Scatter and line plots show time courses for the group averages ($n = 5$) of sensitivity to von Frey (a) and Pin (b), as well as weight-bearing asymmetry (c, $n = 4$) following ipsilateral subepineural sciatic nerve injection (SSNI) of TTA-P2 (100 μg, 100 μl) or saline (100 μl), determined at day 35 after MIA-OA induction. Right panels show averaged area under the curve (AUC) calculated for each individual for 1 h period (15 min interval) following injection for von Frey, Pin, and weight-bearing tests, respectively. Behavior tests at 35 days before injection were used as the treatment baseline values for AUC calculation. $^{\#\#}p < 0.01$ for comparison to treatment BL and $^*p < 0.05$, $^{**}p < 0.01$, and $^{***}p < 0.001$ for comparison between groups after treatment, respectively (repeated measures two-way ANOVA and post-hoc analysis with Bonferroni test for von Frey and weight bearing, and nonparametric analyses by Friedman's test with Dunn's post hoc for Pin. $^*p < 0.05$ and $^{***}p < 0.001$ for AUC comparison between groups (two-tailed unpaired Student's t tests).

Therefore, conceivably, the inflammatory responses and sensory neuron damage may also play pathological roles for upregulation of $Ca_V3.2$ in the context of MIA OA model since the function and expression of $Ca_V3.2$ are modulated by a variety of inflammatory and nerve injury mediators.[20,57,69] For example, increased nerve growth factor and tumor necrosis factor-α are common pathological mediators in both neuropathic pain and OA pain, and both are known determinants of regulating T-type Ca^{2+} channels.[10,20,51,69] These processes may cause

peripheral and central sensitization and promote the persistence of neuropathic-like pain in MIA OA model.[70]

The decrease in pain sensation after peripheral injection of TTA-P2 adds further evidence for involvement of peripheral $Ca_V3.2$ activation in MIA OA pain. Previous studies have shown that acute anti-nociception to mechanical stimulation after SN perineural, intrathecal (i.t), or intraperitoneal (i.p) application of TTA-P2 is an effective approach in addressing enhanced $Ca_V3.2$ responses in animal models of both inflammatory and neuropathic pain, with the additional advantage that applied TTA-P2 exerts antinociceptive effects without motor impairment.[40,53,59] T-type $Ca_V3.2$ channels are abundantly expressed in PSN somata and transported to peripheral and central axons where $Ca_V3.2$ contributes to pain perception, neuronal excitability, and spinal synaptic plasticity. Since $Ca_V3.2$ is also expressed in SC neurons, it is unclear whether peripheral or central block of $Ca_V3.2$ is best for analgesic efficacy. Our success in producing analgesia by sciatic injection of TTA-P2 suggests that a peripheral site of $Ca_V3.2$ channel action is involved in pain generation. Since our findings showed that elevated expression and function of $Ca_V3.2$ channels are found in PSNs at multiple lumbar segmental levels after MIA injection into the knee, TTA-P2 directly into the large nerve trunks of the SN could act on axonal $Ca_V3.2$ channels directly at the site of injection, or may spread to more central and peripheral sites of action by bulk flow and diffusion longitudinally within the sciatic and associated spinal nerves, or by axonal transport. Indeed, the direct application of drug to the SN can lead to changes in the properties of DRG neurons.[43,71] It is likely that observed TTA-P2 analgesic effect is predominantly due to inhibition on T-type channels, although we cannot rule out the possibility of some effects on alternative molecular targets. Additionally, SN at the midthigh are composed of axonal fibers from sensory, motor, and sympathetic neurons that may also express T-channels[72,73]; thus, the analgesic effect may be partially resulted from T-channel inhibition in those fibers that also play roles in generation of pain behavior.[74,75]

In conclusion, our findings demonstrate an elevated $Ca_V3.2$ expression and enhanced function of PSN-T-type Ca^{2+} channels that may involve joint- and non-joint innervating afferents at the late stage of MIA OA pain, and indicate that PSN-$Ca_V3.2$ is an important DRG determinant of, and a potential therapeutic target for, chronic knee joint pain. Data also suggest that selective targeting of PSN-$Ca_V3.2$ in peripheral nerves could be adapted for clinical use. Further studies are needed to determine involvement of $Ca_V3.2$ channels in other OA pain models.

Declaration of Conflicting Interests

Funding

ORCID iD

Hongwei Yu (iD) https://orcid.org/0000-0003-3029-3644

References

1. Dieppe PA, Lohmander LS. Pathogenesis and management of pain in osteoarthritis. *Lancet* 2005; 365: 965–973.

2. Schmidt MM, Dringen R. Differential effects of iodoacetamide and iodoacetate on glycolysis and glutathione metabolism of cultured astrocytes. *Front Neuroenergetics* 2009; 1: 1.

3. Dimitroulas T, Duarte RV, Behura A, Kitas GD, Raphael JH. Neuropathic pain in osteoarthritis: a review of pathophysiological mechanisms and implications for treatment. *Semin Arthritis Rheum* 2014; 44: 145–154.

4. Lee AS, Ellman MB, Yan D, Kroin JS, Cole BJ, van Wijnen AJ, Im H-J. A current review of molecular mechanisms regarding osteoarthritis and pain. *Gene* 2013; 527: 440–447.

5. Kuyinu EL, Narayanan G, Nair LS, Laurencin CT. Animal models of osteoarthritis: classification, update, and measurement of outcomes. *J Orthop Surg Res* 2016; 11: 19.

6. Malfait AM, Schnitzer TJ. Towards a mechanism-based approach to pain management in osteoarthritis. *Nat Rev Rheumatol* 2013; 9: 654–664.

7. Thakur M, Dickenson AH, Baron R. Osteoarthritis pain: nociceptive or neuropathic? *Nat Rev Rheumatol* 2014; 10: 374–380.

8. Zhu S, Zhu J, Zhen G, Hu Y, An S, Li Y, Zheng Q, Chen Z, Yang Y, Wan M, Skolasky RL, Cao Y, Wu T, Gao B, Yang M, Gao M, Kuliwaba J, Ni S, Wang L, Wu C, Findlay D, Eltzschig HK, Ouyang HW, Crane J, Zhou F-Q, Guan Y, Dong X, Cao X. Subchondral bone osteoclasts induce sensory innervation and osteoarthritis pain. *J Clin Invest* 2019; 129: 1076–1093.

9. Neogi T. The epidemiology and impact of pain in osteoarthritis. *Osteoarthr Cartil* 2013; 21: 1145–1153.

10. Miller RE, Tran PB, Obeidat AM, Raghu P, Ishihara S, Miller RJ, Malfait A-M. The role of peripheral nociceptive neurons in the pathophysiology of osteoarthritis pain. *Curr Osteoporos Rep* 2015; 13: 318–326.

11. McDougall JJ, Bray RC, Sharkey KA. Morphological and immunohistochemical examination of nerves in normal and injured collateral ligaments of rat, rabbit, and human knee joints. *Anat Rec* 1997; 248: 29–39.

12. Hildebrand C, Oqvist G, Brax L, Tuisku F. Anatomy of the rat knee joint and fibre composition of a major articular nerve. *Anat Rec* 1991; 229: 545–555.

13. Conaghan PG, Cook AD, Hamilton JA, Tak PP. Therapeutic options for targeting inflammatory osteoarthritis pain. *Nat Rev Rheumatol* 2019; 15: 355–363.

14. Lockwood SM, Lopes DM, McMahon SB, Dickenson AH. Characterisation of peripheral and central components of the rat monoiodoacetate model of osteoarthritis. *Osteoarthr Cartil* 2019; 27: 712–722.

15. Fingleton C, Smart K, Moloney N, Fullen BM, Doody C. Pain sensitization in people with knee osteoarthritis: a systematic review and meta-analysis. *Osteoarthr Cartil* 2015; 23: 1043–1056.

16. Arendt-Nielsen L, Nie H, Laursen MB, Laursen BS, Madeleine P, Simonsen OH, Graven-Nielsen T. Sensitization in patients with painful knee osteoarthritis. *Pain* 2010; 149: 573–581.

17. Eitner A, Hofmann GO, Schaible HG. Mechanisms of osteoarthritic pain. Studies in humans and experimental models. *Front Mol Neurosci* 2017; 10: 349.

18. Todorovic SM, Jevtovic-Todorovic V. T-type voltage-gated calcium channels as targets for the development of novel pain therapies. *Br J Pharmacol* 2011; 163: 484–495.

19. François A, Schüetter N, Laffray S, Sanguesa J, Pizzoccaro A, Dubel S, Mantilleri A, Nargeot J, Noël J, Wood JN, Moqrich A, Pongs O, Bourinet E. The low-threshold calcium channel Cav3.2 determines low-threshold mechanoreceptor function. *Cell Rep* 2015; 10: 370–382.

20. Bourinet E, Francois A, Laffray S. T-type calcium channels in neuropathic pain. *Pain* 2016; 157: S15–22.

21. Shao Y, Alicknavitch M, Farach-Carson MC. Expression of voltage sensitive calcium channel (VSCC) L-type Cav1.2 (alpha1C) and T-type Cav3.2 (alpha1H) subunits during mouse bone development. *Dev Dyn* 2005; 234: 54–62.

22. Srinivasan PP, Parajuli A, Price C, Wang L, Duncan RL, Kirn-Safran CB. Inhibition of T-Type voltage sensitive calcium channel reduces load-induced OA in mice and suppresses the catabolic effect of bone mechanical stress on chondrocytes. *PLoS One* 2015; 10: e0127290.

23. Jarvis MF, Scott VE, McGaraughty S, Chu KL, Xu J, Niforatos W, Milicic I, Joshi S, Zhang Q, Xia Z. A peripherally acting, selective T-type calcium channel blocker, ABT-639, effectively reduces nociceptive and neuropathic pain in rats. *Biochem Pharmacol* 2014; 89: 536–544.

24. Felson DT. Developments in the clinical understanding of osteoarthritis. *Arthritis Res Ther* 2009; 11: 203.

25. Thakur M, Rahman W, Hobbs C, Dickenson AH, Bennett DL. Characterisation of a peripheral neuropathic component of the rat monoiodoacetate model of osteoarthritis. *PLoS One* 2012; 7: e33730.

26. Im H-J, Kim J-S, Li X, Kotwal N, Sumner DR, van Wijnen AJ, Davis FJ, Yan D, Levine B, Henry JL, Desevré J, Kroin JS. Alteration of sensory neurons and

spinal response to an experimental osteoarthritis pain model. *Arthritis Rheum* 2010; 62: 2995–3005.

27. Fischer G, Kostic S, Nakai H, Park F, Sapunar D, Yu H, Hogan Q. Direct injection into the dorsal root ganglion: technical, behavioral, and histological observations. *J Neurosci Methods* 2011; 199: 43–55.

28. Bove SE, Calcaterra SL, Brooker RM, Huber CM, Guzman RE, Juneau PL, Schrier DJ, Kilgore KS. Weight bearing as a measure of disease progression and efficacy of anti-inflammatory compounds in a model of monosodium iodoacetate-induced osteoarthritis. *Osteoarthritis Cartilage* 2003; 11: 821–830.

29. Wu HE, Gemes G, Zoga V, Kawano T, Hogan QH. Learned avoidance from noxious mechanical simulation but not threshold Semmes Weinstein filament stimulation after nerve injury in rats. *J Pain* 2010; 11: 280–286.

30. Mapp PI, Sagar DR, Ashraf S, Burston JJ, Suri S, Chapman V, Walsh DA. Differences in structural and pain phenotypes in the sodium monoiodoacetate and meniscal transection models of osteoarthritis. *Osteoarthritis Cartilage* 2013; 21: 1336–1345.

31. Haywood AR, Hathway GJ, Chapman V. Differential contributions of peripheral and central mechanisms to pain in a rodent model of osteoarthritis. *Sci Rep* 2018; 8: 7122.

32. Yu H, Fischer G, Jia G, Reiser J, Park F, Hogan QH. Lentiviral gene transfer into the dorsal root ganglion of adult rats. *Mol Pain* 2011; 7: 63.

33. Jacus MO, Uebele VN, Renger JJ, Todorovic SM. Presynaptic Cav3.2 channels regulate excitatory neurotransmission in nociceptive dorsal horn neurons. *J Neurosci* 2012; 32: 9374–9382.

34. Yu H, Fischer G, Ferhatovic L, Fan F, Light AR, Weihrauch D, Sapunar D, Nakai H, Park F, Hogan QH. Intraganglionic AAV6 results in efficient and long-term gene transfer to peripheral sensory nervous system in adult rats. *PLoS One* 2013; 8: e61266.

35. Corder G, Siegel A, Intondi AB, Zhang X, Zadina JE, Taylor BK. A novel method to quantify histochemical changes throughout the mediolateral axis of the substantia gelatinosa after spared nerve injury: characterization with TRPV1 and substance P. *J Pain* 2010; 11: 388–398.

36. Sonnemann KJ, Heun-Johnson H, Turner AJ, Baltgalvis KA, Lowe DA, Ervasti JM. Functional substitution by TAT-utrophin in dystrophin-deficient mice. *PLoS Med* 2009; 6: e1000083.

37. Liu Z, Wang F, Fischer G, Hogan QH, Yu H. Peripheral nerve injury induces loss of nociceptive neuron-specific galphai-interacting protein in neuropathic pain rat. *Mol Pain* 2016; 12: 174480691664638.

38. Xiang H, Xu H, Fan F, Shin SM, Hogan QH, Yu H. Glial fibrillary acidic protein promoter determines transgene expression in satellite glial cells following intraganglionic adeno-associated virus delivery in adult rats. *J Neurosci Res* 2018; 93: 436–448.

39. Pan B, Guo Y, Wu H-E, Park J, Trinh VN, Luo ZD, Hogan QH. Thrombospondin-4 divergently regulates voltage-gated Ca2+ channel subtypes in sensory neurons after nerve injury. *Pain* 2016; 157: 2068–2080.

40. Choe W, Messinger RB, Leach E, Eckle V-S, Obradovic A, Salajegheh R, Jevtovic-Todorovic V, Todorovic SM. TTA-P2 is a potent and selective blocker of T-type calcium channels in rat sensory neurons and a novel antinociceptive agent. *Mol Pharmacol* 2011; 80: 900–910.

41. Moayeri N, Groen GJ. Differences in quantitative architecture of sciatic nerve may explain differences in potential vulnerability to nerve injury, onset time, and minimum effective anesthetic volume. *Anesthesiology* 2009; 111: 1128–1134.

42. Estebe JP, Myers RR. Amitriptyline neurotoxicity: dose-related pathology after topical application to rat sciatic nerve. *Anesthesiology* 2004; 100: 1519–1525.

43. Flinspach M, Xu Q, Piekarz AD, Fellows R, Hagan R, Gibbs A, Liu Y, Neff RA, Freedman J, Eckert WA, Zhou M, Bonesteel R, Pennington MW, Eddinger KA, Yaksh TL, Hunter M, Swanson RV, Wickenden AD. Insensitivity to pain induced by a potent selective closed-state Nav1.7 inhibitor. *Sci Rep* 2017; 7: 39662.

44. Ferreira-Gomes J, Adaes S, Sarkander J, Castro-Lopes JM. Phenotypic alterations of neurons that innervate osteoarthritic joints in rats. *Arthritis Rheum* 2010; 62: 3677–3685.

45. Nwosu LN, Mapp PI, Chapman V, Walsh DA. Relationship between structural pathology and pain behaviour in a model of osteoarthritis (OA). *Osteoarthritis Cartilage* 2016; 24: 1910–1917.

46. Havelin J, Imbert I, Cormier J, Allen J, Porreca F, King T. Central sensitization and neuropathic features of ongoing pain in a rat model of advanced osteoarthritis. *J Pain* 2016; 17: 374–382.

47. Braz JM, Basbaum AI. Differential ATF3 expression in dorsal root ganglion neurons reveals the profile of primary afferents engaged by diverse noxious chemical stimuli. *Pain* 2010; 150: 290–301.

48. Averill S, Michael GJ, Shortland PJ, Leavesley RC, King VR, Bradbury EJ, McMahon SB, Priestley JV. NGF and GDNF ameliorate the increase in ATF3 expression which occurs in dorsal root ganglion cells in response to peripheral nerve injury. *Eur J Neurosci* 2004; 19: 1437–1445.

49. Mousseau M, Burma NE, Lee KY, Leduc-Pessah H, Kwok CHT, Reid AR, O'Brien M, Sagalajev B, Stratton JA, Patrick N, Stemkowski PL, Biernaskie J, Zamponi GW, Salo P, McDougall JJ, Prescott SA, Matyas JR, Trang T. Microglial pannexin-1 channel activation is a spinal determinant of joint pain. *Sci Adv* 2018; 4: eaas9846.

50. Sagar DR, Burston JJ, Hathway GJ, Woodhams SG, Pearson RG, Bennett AJ, Kendall DA, Scammell BE, Chapman V. The contribution of spinal glial cells to chronic pain behaviour in the monosodium iodoacetate model of osteoarthritic pain. *Mol Pain* 2011; 7: 1744-8069-7-88.

51. Orita S, Ishikawa T, Miyagi M, Ochiai N, Inoue G, Eguchi Y, Kamoda H, Arai G, Toyone T, Aoki Y, Kubo T, Takahashi K, Ohtori S. Pain-related sensory innervation in monoiodoacetate-induced osteoarthritis in rat knees that gradually develops neuronal injury in addition to inflammatory pain. *BMC Musculoskelet Disord* 2011; 12: 134.

52. Wu Q, Henry JL. Delayed onset of changes in soma action potential genesis in nociceptive A-beta DRG neurons in vivo in a rat model of osteoarthritis. *Mol Pain* 2009; 5: 57.

53. Joksimovic SL, Joksimovic SM, Tesic V, Garcia-Caballero A, Feseha S, Zamponi GW, Jevtovic-Todorovic V, Todorovic SM. Selective inhibition of CaV3.2 channels reverses hyperexcitability of peripheral nociceptors and alleviates postsurgical pain. *Sci Signal* 2018; 11: eaao442.

54. Nelson MT, Joksovic PM, Perez-Reyes E, Todorovic SM. The endogenous redox agent L-cysteine induces T-type Ca2+ channel-dependent sensitization of a novel subpopulation of rat peripheral nociceptors. *J Neurosci* 2005; 25: 8766–8775.

55. Li Y, Tatsui CE, Rhines LD, North RY, Harrison DS, Cassidy RM, Johansson CA, Kosturakis AK, Edwards DD, Zhang H, Dougherty PM. Dorsal root ganglion neurons become hyperexcitable and increase expression of voltage-gated T-type calcium channels (Cav3.2) in paclitaxel-induced peripheral neuropathy. *Pain* 2017; 158: 417–429.

56. Rose KE, Lunardi N, Boscolo A, Dong X, Erisir A, Jevtovic-Todorovic V, Todorovic SM. Immunohistological demonstration of CaV3.2 T-type voltage-gated calcium channel expression in soma of dorsal root ganglion neurons and peripheral axons of rat and mouse. *Neuroscience* 2013; 250: 263–274.

57. Watanabe M, Ueda T, Shibata Y, Kumamoto N, Shimada S, Ugawa S. Expression and regulation of Cav3.2 T-Type calcium channels during inflammatory hyperalgesia in mouse dorsal root ganglion neurons. *PLoS One* 2015; 10: e0127572.

58. Marger F, Gelot A, Alloui A, Matricon J, Ferrer JFS, Barrère C, Pizzoccaro A, Muller E, Nargeot J, Snutch TP, Eschalier A, Bourinet E, Ardid D. T-type calcium channels contribute to colonic hypersensitivity in a rat model of irritable bowel syndrome. *Proc Natl Acad Sci USA* 2011; 108: 11268–11273.

59. Chen W, Chi Y-N, Kang X-J, Liu Q-Y, Zhang H-L, Li Z-H, Zhao Z-F, Yang Y, Su L, Cai J, Liao F-F, Yi M, Wan Y, Liu F-Y. Accumulation of Cav3.2 T-type calcium channels in the uninjured sural nerve contributes to neuropathic pain in rats with spared nerve injury. *Front Mol Neurosci* 2018; 11: 24.

60. Kang X-J, Chi Y-N, Chen W, Liu F-Y, Cui S, Liao F-F, Cai J, Wan Y. Increased expression of CaV3.2 T-type calcium channels in damaged DRG neurons contributes to neuropathic pain in rats with spared nerve injury. *Mol Pain* 2018; 14: 1744806918765808.

61. Ayoola C, Hwang SM, Hong SJ, Rose KE, Boyd C, Bozic N, Park J-Y, Osuru HP, DiGruccio MR, Covey DF, Jevtovic-Todorovic V, Todorovic SM. Inhibition of CaV3.2 T-type calcium channels in peripheral sensory neurons contributes to analgesic properties of epipregnanolone. *Psychopharmacology (Berl)* 2014; 231: 3503–3515.

62. Todorovic SM, Jevtovic-Todorovic V. Targeting of CaV3.2 T-type calcium channels in peripheral sensory neurons for the treatment of painful diabetic neuropathy. *Pflugers Arch* 2014; 466: 701–706.

63. Latham JR, Pathirathna S, Jagodic MM, Choe WJ, Levin ME, Nelson MT, Lee WY, Krishnan K, Covey DF, Todorovic SM, Jevtovic-Todorovic V. Selective T-type calcium channel blockade alleviates hyperalgesia in ob/ob mice. *Diabetes* 2009; 58: 2656–2665.

64. Tomita S, Sekiguchi F, Deguchi T, Miyazaki T, Ikeda Y, Tsubota M, Yoshida S, Nguyen HD, Okada T, Toyooka N, Kawabata A. Critical role of Cav3.2 T-type calcium channels in the peripheral neuropathy induced by bortezomib, a proteasome-inhibiting chemotherapeutic agent, in mice. *Toxicology* 2019; 413: 33–39.

65. Wu Q, Henry JL. Changes in abeta non-nociceptive primary sensory neurons in a rat model of osteoarthritis pain. *Mol Pain* 2010; 6: 37.

66. Miller RE, Kim YS, Tran PB, Ishihara S, Dong X, Miller RJ, Malfait A-M. Visualization of peripheral neuron sensitization in a surgical mouse model of osteoarthritis by in vivo calcium imaging. *Arthritis Rheumatol* 2018; 70: 88–97.

67. O'Neill TW, Felson DT. Mechanisms of osteoarthritis (OA) pain. *Curr Osteoporos Rep* 2018; 16: 611–616.

68. Feng X-J, Ma L-X, Jiao C, Kuang H-X, Zeng F, Zhou X-Y, Cheng X-E, Zhu M-Y, Zhang D-Y, Jiang C-Y, Liu T. Nerve injury elevates functional Cav3.2 channels in superficial spinal dorsal horn. *Mol Pain* 2019; 15: 1744806919836569.

69. Sekiguchi F, Tsubota M, Kawabata A. Involvement of voltage-gated calcium channels in inflammation and inflammatory pain. *Biol Pharm Bull* 2018; 41: 1127–1134.

70. Ren K, Dubner R. Interactions between the immune and nervous systems in pain. *Nat Med* 2010; 16: 1267–1276.

71. DiStefano PS, Friedman B, Radziejewski C, Alexander C, Boland P, Schick CM, Lindsay RM, Wiegand SJ. The neurotrophins BDNF, NT-3, and NGF display distinct patterns of retrograde axonal transport in peripheral and central neurons. *Neuron* 1992; 8: 983–993.

72. Kisiswa L, Erice C, Ferron L, Wyatt S, Osorio C, Dolphin AC, et al. T-type Ca2+ channels are required for enhanced sympathetic axon growth by TNFalpha reverse signalling. *Open Biol* 2017; 7: 160288.

73. Westenbroek RE, Hoskins L, Catterall WA. Localization of Ca2+ channel subtypes on rat spinal motor neurons, interneurons, and nerve terminals. *J Neurosci* 1998; 18: 6319–6330.

74. Schlereth T, Birklein F. The sympathetic nervous system and pain. *Neuromolecular Med* 2008; 10: 141–147.

75. Boadas-Vaello P, Castany S, Homs J, Álvarez-Pérez B, Deulofeu M, Verdú E. Neuroplasticity of ascending and descending pathways after somatosensory system injury: reviewing knowledge to identify neuropathic pain therapeutic targets. *Spinal Cord* 2016; 54: 330–340.